MICHIGAN STATE
UNIVERSITY

National Superconducting Cyclotron Laboratory

g FACTORS OF THE FIRST 2^+ STATES IN THE TRANSITIONAL ^{92,94,96,98,100}Mo ISOTOPES AND THE ONSET OF COLLECTIVITY

P.F. MANTICA, A.E. STUCHBERY, D.E. GROH,
J.I. PRISCIANDARO, and M.P. ROBINSON

MSUCL-1186

DECEMBER 2000

g Factors of the first 2^+ states in the transitional ^{92,94,96,98,100}Mo isotopes and the onset of collectivity

P.F. Mantica, [1,2] A.E. Stuchbery, [3] D.E. Groh, [1,2] J.I. Prisciandaro, [1,2] and M.P. Robinson[3]
[1] *National Superconducting Cyclotron Laboratory, Michigan State University, East Lansing, MI 48824*
[2] *Department of Chemistry, Michigan State University, East Lansing, MI 48824*
[3] *Department of Nuclear Physics, Research School of Physical Sciences and Engineering, Australian National University, Canberra, ACT 0200, Australia*
(November 17, 2000)

Abstract

The g factors of the 2_1^+ states of the stable, even-even Mo isotopes ^{92,94,96,98,100}Mo were measured using the transient field method. While ^{92}Mo$_{50}$ has a g factor consistent with that of the $\pi g_{9/2}^2$ configuration, the g factor of ^{94}Mo is about 60% of the hydrodynamic model value, Z/A. As further pairs of neutrons are added, the heavier isotopes ^{96,98,100}Mo show a monotonic increase in $g(2^+)$ to values that exceed Z/A for ^{98}Mo and ^{100}Mo. The systematic behavior of the $g(2_1^+)$ values for the Mo isotopes, as one moves away from the neutron shell closure at $N = 50$, is compared with the shell model, a collective model with pairing corrections and IBM-2 calculations.

21.10.Ky,21.60.Cs,23.20.En,27.60.+j

I. INTRODUCTION

The low-energy structure of the even-even Mo ($Z = 42$) isotopes undergoes a change from spherical at the neutron-closed shell nucleus $^{92}Mo_{50}$ to rotational-like at $^{104}Mo_{62}$, for which $E(2_1^+) = 192$ keV and $E(2_1^+)/E(4_1^+) = 2.91$. In addition, the excited 0^+ state observed at an energy near the 2_1^+ state in both ^{98}Mo and ^{100}Mo is a signature of shape-coexistence. Toward the proton drip line, the $E(2_1^+)$ values drop dramatically from 1510 keV in ^{92}Mo to 444 keV in $^{84}Mo_{42}$, the lightest even-even isotope of molybdenum for which γ-ray data are available [1]. The systematics of the low-energy 0^+, 2^+, and 4^+ levels in the even-even Mo isotopes are given in Fig. 1.

The shell model has been applied quite extensively to the Zr and Mo isotopes near $N = 50$. Pioneering work was performed by Talmi and Unna [2], Auerbach and Talmi [3] and Vervier [4] in the 1960s. Model spaces with a few orbits outside $^{88}_{38}Sr_{50}$ or $^{90}_{40}Zr_{50}$ cores were considered. In the mid-1970s Gloeckner [5] determined effective interactions for the Zr and Nb isotopes with ^{88}Sr taken as an inert core and protons filling the $(2p_{1/2}, 1g_{9/2})$ levels and neutrons in the $(2d_{5/2}, 3s_{1/2})$ levels. There has been ongoing interest up to the present time. For example, very recently Zhang *et al.* [6] have studied nuclei with $N \geq 50$ and $A = 92$-98 in the larger model space $\pi(1f_{5/2}, 2p_{3/2}, 2p_{1/2}, 1g_{9/2})$ and ν $(1g_{9/2}, 2p_{1/2}, 2d_{5/2}, 3s_{1/2}, 2d_{3/2}, 1g_{7/2})$, and Holt *et al.* [7] have considered the zirconium isotopes between ^{90}Zr and ^{100}Zr with a large basis and realistic effective interactions. Also recently, Johnstone and Towner have calculated effective charges in the mass 90 region [8], and Lisetskiy *et al.* [9] have performed shell model calculations for ^{94}Mo to investigate the nature of states assigned mixed-symmetry in the proton-neutron interacting boson model.

A feature of the level spectra of the even Zr and Mo isotopes near $N = 50$ that has been emphasized [6,7], is the apparent weak-coupling of the proton and neutron valence spaces. From the level spectrum alone, however, one cannot judge whether the coupling is weak or rather strong and state-independent. Certainly, the evolution of collective structures implies increasing coupling between the proton and neutron excitations as the number of valence neutrons increases. Magnetic moments can probe this coupling through their sensitivity to the relative contributions of protons and neutrons to the angular momentum of the states.

The transitional nature of the molybdenum isotopes away from $N = 50$ has been the focus of several theoretical efforts. Federman and Pittel [10] carried out Hartree-Fock Bogoliubov calculations to explore the role of the neutron-proton interaction in inducing deformation in the Zr-Mo region around $A = 100$. They used an inert $^{94}_{38}Sr_{56}$ core and considered the single-particle proton orbitals $2p_{1/2}$, $1g_{9/2}$, and $2d_{5/2}$ and neutron orbitals $3s_{1/2}$, $2d_{3/2}$, $1g_{7/2}$, and $1h_{11/2}$. The single particle energies were determined for $^{88}Sr_{50}$ and then corrected to account for the additional six neutrons in the $2d_{5/2}$ orbital. The transition to more deformed structures at $N = 60$ in both zirconium and molybdenum nuclei was attributed to a strong $\nu g_{7/2}$ - $\pi g_{9/2}$ neutron-proton interaction as neutrons filled the $1g_{7/2}$ orbital beyond $N = 56$.

Khasa, Tripathi, and Sharma [11] also systematically studied the low-energy structure of the transitional, even-even Mo isotopes within the shell model using a pairing plus quadrupole-quadrupole effective interaction. Starting with a $^{76}Sr_{38}$ inert core, their basis set included the proton and neutron orbitals $2p_{1/2}$, $3s_{1/2}$, $2d_{3/2}$, $2d_{5/2}$, $1g_{7/2}$, $1g_{9/2}$, and $1h_{11/2}$. The $2p_{1/2}$ orbital was included to probe the effects of a $N = 40$ subshell closure on the low-energy structure of the molybdenum isotopes.

Heyde *et al.* [12] have studied the intruder nature of the low-energy 0^+ states in the even-even Mo isotopes within the shell model. They emphasize the effects of (i) a strong monopole interaction between the $\nu g_{7/2}$ and $\pi g_{9/2}$ orbitals and (ii) a large quadrupole-quadrupole correction within the valence neutron shell $N = 56 - 82$ on the low-energy structure of the transitional Mo isotopes.

The concept of configuration mixing in the molybdenum isotopes was pursued by Sambataro and Molnar [13], who used two different boson configurations within the interacting boson model (IBM-2) to reproduce the low-energy level structure of the Mo isotopes through the transition region $A = 96 - 104$. The first configuration assumed one proton boson ($N_\pi = 1$) outside a $Z = 40$ closed shell, while the second considered the promotion of one proton-boson from below the $Z = 40$ shell closure, resulting in a total of three proton bosons ($N_\pi = 3$: two proton-particle bosons and one proton-hole boson). Neutron particle bosons were counted with reference to the $N = 50$ closed shell for each molybdenum isotope. Strong mixing was calculated for ^{98}Mo and ^{100}Mo. The ground state of ^{98}Mo was mostly $N_\pi = 1$, while for ^{100}Mo the wavefunction within the configuration $N_\pi = 3$ was predominant. The favoring of the configuration $N_\pi = 3$ above $N = 56$ is suggested to be a result of a strong neutron-proton $\nu g_{7/2}$ - $\pi g_{9/2}$ interaction, as discussed in Ref. [10].

As an alternative to configuration mixing calculations within the IBM-2, Cata *et al.* [14] investigated the effects of proton-neutron interactions on the low-energy levels of the even-even Mo isotopes using the IBM-1 and an effective boson number derived from previous IBM-2 parametrizations [13] and from $N_\pi N_\nu$ systematics [15]. Although the IBM-1 calculations reproduced the general features of the IBM-2 calculations with configuration mixing [13], the microscopic relationship between the effective boson number and neutron-proton interaction strength was not explored in detail. Dejbakhsh *et al.* [16] also considered an alternative to configuration mixing calculations for the Mo isotopes in the IBM-2 by employing different relative d-boson energies, ϵ_π, for protons and ϵ_ν, for neutrons. Considering two proton bosons outside a $Z = 38$ closed shell, or four proton hole bosons in a $Z = 50$ closed shell, their IBM-2 calculations with $\epsilon_\pi \neq \epsilon_\nu$ reproduced well the low-energy levels and E2 transition rates of the even-even Mo isotopes around $A = 100$.

It is evident that a variety of theoretical approaches can reproduce the energy spectra of these transitional isotopes while the microscopic connection between the models is not always clear. Hence, to learn more about the single-particle structures underlying the emerging low-energy collective properties of the even-even molybdenum isotopes in the transition region between $A = 90$ and $A = 100$, we have measured the g factors of the first 2^+ states of the stable, even-even isotopes ^{92,94,96,98,100}Mo.

Some information on the g factors of 2_1^+ states in the even-even molybdenum isotopes is available in the literature. The average g factor for the first 2^+ states in ^{98,100}Mo was deduced to be 0.34(18) by Heestand *et al.* [17] from early ion implantation-perturbed angular correlation measurements. This was a 'thick-foil' measurement in which the Mo nuclei experienced both static and transient fields. The transient field was not well characterized at the time, so the result must be taken as tentative. The individual g factors for the 2_1^+ states in the stable, even-even isotopes of molybdenum were measured in an early transient field study at Chalk River [18,19]. This transient field measurement employed a sequence of targets of isotopically enriched Mo $\sim$0.7 mg/cm^2 thick, followed by 3.6 - 4.0 mg/cm^2 thick annealed Fe foils with Cu backings. A 130 MeV ^{40}Ca beam was used to Coulomb excite the

Mo target nuclei. The g factors, deduced from consecutive measurements, had errors in the range 14 – 17%; these errors include statistical uncertainties and systematic uncertainties in the transient field calibration, the recoil energy loss, and the slope of the angular correlation. As systematic errors can occur through the consecutive use of a sequence of different targets, a new set of simultaneous measurements is required.

Menzen *et al.* [20] have deduced the g factors of the first excited 2^+ levels in β unstable ^{102,104}Mo by measuring the perturbed angular correlations for $\gamma\gamma$ cascades in the $0_2^+ \to 2_1^+ \to 0_1^+$ level sequence. The apparently different g factors for the 2_1^+ states in ^{102}Mo ($g = 0.42\pm0.07$) and ^{104}Mo ($g = 0.19^{+0.12}_{-0.11}$) were considered not to deviate significantly from the vibrational-rotational model predictions of Greiner [21] (i.e. 0.34 and 0.32, respectively). The $g(2_1^+)$ values for ^{102,104}Mo were also used to extract an average proton boson g factor $\langle g_\pi^{\rm ave}\rangle = 1.00(23)$ for the $A = 100$ region based on an IBM-2 parametrization of $g(2^+)$ and assuming $g_\nu = 0$, where g_ν is the neutron boson g factor.

II. EXPERIMENTAL TECHNIQUE

The transient field technique [22] was used to determine the g factors of the first excited states of the stable, even-even molybdenum isotopes, ^{92,94,96,98,100}Mo. A beam of 100 MeV $^{32}S^{8+}$ from the 14UD Pelletron accelerator at Australian National University, having an average current of 30 enA, was made incident upon a multilayered target consisting of 0.757 mg/cm^2 $^{\rm nat}$Mo, 2.57 mg/cm^2 $^{\rm nat}$Fe, and a 'thick' (7.6 mg/cm^2) Cu backing foil. The target was prepared by first sputtering natural molybdenum onto one side of the annealed Fe foil, followed by evaporation of Cu onto the opposite side of the same Fe foil. The ^{32}S beam entered the molybdenum side of the target, Coulomb exciting Mo nuclei. The resulting Mo γ rays were detected using four high purity Ge detectors placed at $\theta_\gamma = \pm65°$ and $\theta_\gamma = \pm115°$ relative to the incident beam direction. The $+65°$ and $-65°$ detectors were placed 7.3 cm and 6.7 cm, respectively, from the target position, to match their solid-angles, while the two backward detectors were each placed 8.7 cm from this location. Particle-γ-ray correlations were measured by detecting the Mo γ rays in coincidence with backscattered ^{32}S ions which entered an annular Si detector covering an angular range from 150° to 167°, again relative to the incident beam direction.

The Fe layer of the target was polarized by an external field of ≈ 0.08 T, the direction of which was reversed automatically, approximately every 20 min, to minimize possible systematic errors. The energies and velocities with which the Mo ions entered and exited the Fe layer, as calculated with the stopping powers of Ziegler, Biersack, and Littmark [23], are presented in Table I. After leaving the ferromagnetic foil, the Mo nuclei were stopped in the Cu backing where they experience no further magnetic perturbations. The Fe foil magnetization was measured with the Rutgers magnetometer [27] to be $M = 0.163(3)$ T for a polarizing field of $B_{\rm ext} = 0.04$ T, $M = 0.168(3)$ T for a polarizing field of $B_{\rm ext} = 0.06$ T, and consistent with the full saturation value of $M = 0.171$ T at 300 K for $B_{\rm ext} = 0.08$ T.

The precession angle of the Mo nuclei due to the interaction of their magnetic moments with the transient hyperfine field in the Fe foil is

$$\Delta\theta = g\phi, \tag{1}$$

where g is the nuclear g factor and ϕ is the integral strength of the transient field

$$\phi = -\frac{\mu_N}{\hbar} \int_{T_1}^{T_2} B_{\mathrm{tr}}(t) \mathrm{e}^{-t/\tau}\, \mathrm{d}t, \tag{2}$$

and the times T_1 and T_2 are the entrance and exit times, respectively, for a Mo ion crossing the Fe foil. The strength of the transient field for a Mo ion in Fe, B_{tr}, varies with time as the ion slows in the foil. This effective field strength ϕ is insensitive to the level lifetime, τ, provided the lifetime is longer than the transit time, i.e. $\tau > T_2 - T_1$; however ϕ is reduced if τ is of the same order or shorter than the transit time through the ferromagnetic layer. (In the present work this is the case only for ^{92}Mo.)

The experimental precession angle is related to the field up/down counting asymmetry ϵ by the expression

$$\Delta\theta = \frac{\epsilon}{S}, \tag{3}$$

where S is the logarithmic derivative of the angular correlation at the detection angle θ_γ and

$$\epsilon = \frac{1-\rho}{1+\rho}. \tag{4}$$

The 'double ratio' ρ is related to the counting rates in the detectors at $\pm\theta_\gamma$, $N(\pm\theta_\gamma)$, for field up ($\uparrow$) and down ($\downarrow$) conditions by

$$\rho = \sqrt{\frac{N(+\theta_\gamma)\uparrow N(-\theta_\gamma)\downarrow}{N(+\theta_\gamma)\downarrow N(-\theta_\gamma)\uparrow}}. \tag{5}$$

Unperturbed particle-γ-ray angular correlations for the $2^+ \to 0^+$ transitions in each Mo nucleus were calculated using a version of the Winther-de Boer Coulomb exitation code [28]. These calculations considered the finite angular coverage of the particle detector, the beam energy loss in the target, and feeding from populated higher-excited states. Relevant matrix elements for the Coulomb excitation calculations were taken from Ref. [29]. To confirm the angular correlation calculations, the unperturbed particle-γ-ray angular correlations were also measured for the two forward detectors. These detectors were successively placed at angles 0°, ±30°, ±45°, ±55°, ±60°, and ±65°, while the backward detectors were kept at ±115° and used for normalization.

III. RESULTS

A γ-ray spectrum collected at −65° to the beam direction in coincidence with backscattered ^{32}S ions following Coulomb excitation of the $^{\mathrm{nat}}$Mo target is shown in Fig. 2. This spectrum represents all of the data collected at this detector position for both field up and field down conditions. All γ-ray transitions in this spectrum can be attributed to known transitions in the stable molybdenum isotopes. The γ rays de-exciting the 2_1^+ states in ^{96}Mo and ^{98}Mo, with energies 778 and 786 keV, respectively, were readily resolved in each of the four γ-ray spectra. A significant Doppler broadening was observed for the $2_1^+ \to 0_1^+$ transition in ^{92}Mo due to the relatively short mean lifetime ($\tau = 537$ fs [30]) of the 2_1^+ state. The intensities of the observed feeding transitions to the first excited 2^+ states in the even-even Mo isotopes were consistent with results from our Coulomb excitation calculations.

The measured and calculated unperturbed particle-γ-ray angular correlations for the $2_1^+ \rightarrow 0_1^+$ transitions in ^{94,96,98,100}Mo are shown in Fig. 3. The fitted angular correlation data confirm that the Ge detectors in the forward beam direction were indeed at the nominal angles at which they were positioned. They also corroborate the statistical tensors extracted from the Coulomb excitation calculations. The counting asymmetries, S values, and measured precession angles for the forward and backward detector pairs are presented in Table II. Cascade feeding corrections to the statistical tensors become more significant with increasing neutron number. For example, in comparison with ^{92}Mo, ^{100}Mo shows a 25% change in the logarithmic derivative of the angular correlation, S, for both forward and backward detectors, which can be attributed to substantial feeding of the 2_1^+ state from the higher-energy 4_1^+, 2_2^+, and 0_1^+ states. As feeding corrections only become significant for the heavier, more collective isotopes, we have analyzed the data assuming that the average g factor of the feeding states is the same as that of the fed 2_1^+ state. The extracted g factors are not sensitive to this assumption to any significant extent.

To extract the g factors for the 2_1^+ states from the measured precession angles, knowledge of the integral strength of the transient field for Mo ions traversing magnetized Fe is needed. Stuchbery *et al.* [26] found that the transient field for Pd ions recoiling through magnetized Fe can be described by

$$B(Z,v) = a\ Z\ (v/v_0)^p, \tag{6}$$

where $a = 21.5 \pm 3.5$ Tesla and $p = 0.41 \pm 0.15$. In a subsequent study using the transient field method and an Fe foil that was the same thickness as the one used in the present work, precession angles were measured for the first 2^+ states in three even-even Pd isotopes, ^{106,108,110}Pd, as well as the first $3/2^-$ and $5/2^-$ states in ^{103}Rh [31]. Since the g factors were determined in independent measurements [32–35], experimental ϕ values can be extracted for Pd and Rh in Fe using Eq. 1. We use these data to re-evaluate the parameter a in Eq. 6, adopting $p = 0.41$. As shown in Table III, we obtain $a = 23.65 \pm 1.01$ Tesla. The ϕ values for the Mo 2_1^+ states were therefore calculated with Eq. 2 and the transient field scaling relation given by Eq. 6, with these parameter values. This accounts for the different Z value, as well as the slightly different average velocity with which the Mo ions enter and exit the Fe foil. The field calibration adopted for Mo in Fe is then equivalent to a small extrapolation from the experimental field strengths for Pd and Rh in Fe measured under very similar conditions.

The adopted calibration ϕ values are listed in Table IV, along with the deduced $g(2_1^+)$ values for ^{92,94,96,98,100}Mo. Note that the finite lifetimes of each of the 2_1^+ states, which were taken from the compilation of Raman *et al.* [30], were included in the evaluation of ϕ.

Other scaling relations for the transient field experienced by ions traversing a ferromagnetic host as a function of Z and v/v_0 have been proposed by groups at Rutgers [24] and Chalk River [25]. In Table I, the ϕ values for these parametrizations are compared with predictions of the parametrization proposed for Pd in Fe [26] and the present adopted values that take account of more recent data for Pd and Rh in Fe [31]. Firstly, to estimate the magnitude of the systematic error on the absolute g factors due the ion velocity dependence associated with our choice of transient field parametrization, we calculated the ratios

$\phi(\mathrm{Mo})/\phi(\mathrm{Pd})$ and $\phi(\mathrm{Mo})/\phi(\mathrm{Rh})$ using Eq. 2 with the Rutgers and Chalk River parametrizations in place of that adopted. The extrapolation of the integral transient field strength from Pd to Mo varied by less than 4% between the three parametrizations of the transient field velocity dependence. The agreement in extrapolation from Rh to Mo was even better, of order 2%. This small possible systematic error in the transient field calibration is not included in the error estimates for the absolute g factors reported in Table IV. Secondly, it may be noted from Table I that the different parametrizations agree within $\sim \pm 9\%$ of that adopted, and that the uncertainty in the Rutgers parametrization, for example, due to uncertainties in the parameter values, is about 10%. We are able to assign a smaller error to our absolute g factors because we have calibrated the transient field relative to neighboring nuclei studied under nearly identical conditions.

In the Chalk River measurements [18,19] the transient field parametrization adopted was of the same form as Eq. 6, but with $a = 10.9 \pm 1.0$ T and $p = 1$. It turns out that the integral field strengths obtained in their measurements with their linear-velocity parametrization are almost identical with the non-linear one we adopted. Nevertheless, for a proper comparison, we have re-evaluated the Chalk River results to correspond to our adopted field parameters. Details of the re-evaluation are presented in Table V. We have added an extra 5% to the final uncertainties in these sequential measurements to allow for possible systematic errors due to uncertainties in the thicknesses of the different Fe foils, which magnify uncertainties in the velocity-dependence of the transient field strength, and possible variations in other factors such as the magnetizations of the foils. Table VI shows a comparison of the present and previous g factors.

On the whole, the present g factors for the first excited 2^+ states of the stable, even-even molybdenum isotopes compare favorably with the earlier results of Häusser *et al.* [18,19]. However, the present results reveal a steady increase in the $g(2_1^+)$ values with increasing neutron number in the range $A = 94-100$ that is not apparent from the older measurements. In particular, the previous g factor for ^{100}Mo appears to be smaller than the present value. Given that this state is relatively long lived and that the exit velocity in the Chalk River measurement was rather low, there is a chance that a smaller precession was observed because a fraction of the ^{100}Mo ions stopped in the Fe foil (rather than the Cu backing) where they experience the static hyperfine field which, for Mo in Fe, is $-25.6(5)$ T [37]. On the other hand, this effect on its own is unlikely to fully account for the difference in the measured g factors and the two measurements almost agree within the assigned errors. For the following discussion we therefore adopt g factors that are the average of the present and (re-evaluated) previous work. These values are shown in the final column of Table VI.

IV. DISCUSSION

Häusser *et al.* [18] compared their g factor results with the theoretical calculations of Greiner [21], Kisslinger and Sorenson [38], and Lombard [39]. Greiner's model provides a rough correction to the collective model $g = Z/A$ to include different pairing between protons and neutrons in a given nucleus and cannot meaningfully be applied to the $N = 50$ nucleus ^{92}Mo. For ^{94}Mo and the heavier isotopes, we pursue a more accurate way to correct Z/A for pairing in terms of the Migdal approximation [40] below.

Kisslinger and Sorenson [38], and Lombard [39], both applied pairing plus multipole interactions to study the collective features of even-even nuclei. Given the simplifying assumptions in these models, the results must be considered somewhat schematic. Nevertheless Lombard correctly predicted the fall in g factor value between ^{92}Mo and the heavier isotopes, and the Kisslinger and Sorenson results revealed a monotonic increase in the g(2_1^+) values for the even-even Mo isotopes after ^{92}Mo, although the moments predicted for ^{94}Mo and ^{96}Mo are much too small.

We will discuss our results in terms of several models, beginning with the shell model for the isotopes near ^{92}Mo, and then turning to collective models for the heavier isotopes, namely the Migdal-corrected geometrical model and IBM-2.

A. Shell Model Calculations

As noted in the introduction, there have been several recent shell-model studies of the Zr and Mo isotopes near $N = 50$ [6–8] and attention has been drawn to the apparent weak-coupling of the proton and neutron excitations when a few valence nucleons are added to the $N = 50$ closed shell. While there is now extensive data [41–43] on the magnetic moments in this region, these have not been calculated in recent work. The present calculations were undertaken to examine the magnetic moments predicted by previously proposed interactions, particularly those with limited valence spaces. A comprehensive set of calculations with large basis spaces is beyond the scope of the present work.

Calculations were performed using the code OXBASH [44] for several different basis spaces and interactions. In all calculations the effective charges of the proton and neutron were taken to be $e_\pi^{\text{eff}} = 1.77$ and $e_\nu^{\text{eff}} = 1.19$, consistent with values suggested in Refs. [5,8]. The intrinsic spin g factors of the nucleons were quenched to 0.75 times the bare nucleon values, i.e. $g_s(\pi) = +4.19$, $g_s(\nu) = -2.87$, while the orbital g factors were $g_l = 1(0)$ for protons(neutrons).

Following Vervier [4], we first took ^{90}Zr as the core nucleus and confined the valence nucleons to $\pi 1g_{9/2}$ and $\nu 2d_{5/2}$. Single particle energies were taken from the ground-state binding energies of ^{91}Nb and ^{91}Zr. Effective two-body interactions were determined from the low-excitation energy spectra of ^{92}Mo, ^{92}Zr and ^{92}Nb. The spectra, moments and transition rates were calculated for ^{91,92,94,95}Zr and ^{92,94,95,96}Mo. This calculation represents about the simplest approach one can take. Results are presented in Tables VII and VIII in the column labelled I. Note that a number of states, including some of those for which moment data are available, are outside the model space. (For further comparisons of the level spectra, which are quite well described, see Ref. [4]). We refer to this as Calculation I. The $g(2_1^+)$ predictions of this and the following shell model calculations for ^{92,94}Mo are compared with experimental values in Fig. 4.

Despite the simplicity of the basis, Calculation I qualitatively tracks the main trends in the moment data. In particular, the moments of the 8^+ states in ^{92,94}Mo, which remain nearly pure $\pi(1g_{9/2})^2_{8^+}$ configurations, are close to experiment and the dramatic decrease in the $g(2_1^+)$ value as neutron pairs are added to ^{92}Mo is predicted qualitatively. The difficulties are that (i) the g factors of the low spin states in ^{94,95,96}Mo are too negative, i.e. too close to the pure $\nu(2d_{5/2})^n_{2^+}$ configurations; and (ii) the quadrupole transition rates are increasingly underestimated as the number of valence neutrons increases.

In the second calculation (Calculation II) we applied the basis space and interactions of Gloeckner [5] to ^{90,91,92,94,95,96}Zr and ^{92,94,95,96}Mo. The core was taken as ^{88}Sr, with protons filling the $2p_{1/2}$ and $2g_{9/2}$ obitals and neutrons filling the $2d_{5/2}$ and $3s_{1/2}$ orbitals. The moments and transition rates are shown in the column labelled II in Table VII (Zr) and Table VIII (Mo). Generally, the moments in the Zr isotopes are very well described. The main indication that the basis space is truncated too severely is that the $g(2_1^+)$ values in ^{92,94}Zr are too negative compared with experiment. On the other hand, the 4_1^+ state in ^{94}Zr has a theoretical g factor that agrees very well with experiment.

The description of the magnetic moments and E2 transition rates in the Mo isotopes is much improved compared with Calculation I; the undesired trends in moments and transition rates are much weaker, although still present. As pointed out by Johnstone and Towner [8], a more extended model space for the neutrons, which includes $\nu 2d_{5/2}$, $3s_{1/2}$, $2d_{3/2}$ and $1g_{7/2}$ orbits, is required to get the negative quadrupole moments that are observed experimentally.

In the third case (Calculation III) we used the approach of Zhang *et al.* [6] and applied it to ^{90,91,92}Zr and ^{92,94}Mo. This calculation has a more extended basis space, $\pi(1f_{5/2}, 2p_{3/2}, 2p_{1/2}, 1g_{9/2})$ and ν $(1g_{9/2}, 2p_{1/2}, 2d_{5/2}, 3s_{1/2}, 2d_{3/2}, 1g_{7/2})$, although the proton excitations are constrained by the requirement that no more than two protons can be excited across the $Z = 38$ subshell gap into $\pi 2p_{1/2}$ and $\pi 1g_{9/2}$. It also does not allow particle-hole excitations across the $N = 50$ shell closure. Overall, the calculated moments are in better agreement with experiment, but the improvement is not universal and the $g(2^+)$ values in the $N = 52$ isotones are still underestimated. Simply extending the basis space is clearly not a panacea for the problems with the calculated magnetic moments.

All of the shell model calculations imply a weak coupling between the valence proton and valence neutron excitations, as has been discussed recently [6,7]. It gives rise to the small predicted g factors of the 2_1^+ states in ^{92,94}Zr and ^{94,96}Mo which, in the models, are predominantly (if not pure) $\nu(d_{5/2})^n$ excitations. The measured g factors show that the weak-coupling scenario is only approximately correct for the 2_1^+ states, but seems to become a better approximation at higher spins. In fact, the sharp fall in $g(2_1^+)$ between ^{92}Mo ($N = 50$), for which the 2_1^+ state is essentially a $\pi(g_{9/2})^n$ excitation, and ^{94}Mo ($N = 52$), for which the 2_1^+ state has a dominant $\nu(d_{5/2})^2$ contribution, stems from the weakness of the interaction between the valence protons and neutrons and the fact that valence neutron excitations tend to be favored over valence proton excitations which have a contribution from the repulsive Coulomb interaction. We can conclude that the weak-coupling picture is appropriate, at least approximately, for even the 2_1^+ states. On the other hand, the measured g factors in the $N = 52$ isotones are always nearer to Z/A than predicted by the shell model calculations. The lowest 2_1^+ states can be expected to show more pronounced collective features than the higher-spin states. With this in mind, we estimate the collective g factors of $^{94-104}$Mo in the following subsection.

It is worth noting that the $\nu 2d_{5/2}$ subshell closure is pronounced in the Zr isotopes, making ^{96}Zr a 'quasiclosed-shell' nucleus. In the Mo isotopes, however, the effect of this subshell closure is much more subtle. A vestige of the subshell closure is seen in that the $N = 56$ nucleus ^{98}Mo has a slightly higher 2_1^+ excitation energy than ^{96}Mo, contrary to the marked trend toward more collective and deformed structures beyond ^{100}Mo. From a shell model perspective, the neutron subshell closures at $N = 56$ and $N = 58$ could contribute to the observed maximum g factor values in ^{98,100}Mo by increasing the neutron excitation energies and allowing the protons to carry proportionately more of the spin.

B. Collective g factors in the Migdal approximation

The Migdal approximation [40] has been employed rather successfully to describe the g-factor systematics of collective nuclei in the rare earth region [45]. We have made a similar set of calculations for the ^{94,96,98,100,102,104}Mo isotopes. The pair gaps required were calculated microscopically using the standard Woods-Saxon potential and pairing parameters recommended for this region in Ref. [46]. Since the quadrupole moment data do not extend across all of the isotopes of interest, the deformations were taken from the intrinsic quadrupole moments computed by Möller and Nix [47]. Relevant parameters and results are presented in Table IX. Given the simplicity of this model, the calculated $g(2_1^+)$ values are in very good agreement with experiment (see Fig. 5). In particular, the rise in g value to a maximum at ^{100}Mo is well described. In this model, the g factor tends to increase as the neutron pair-gap, Δ_n, increases and/or the proton pair-gap, Δ_p, decreases. The pair gaps are determined largely by the level density near the Fermi surface. While the behavior of Δ_n reflects the general increase in level density that one would intuitively expect as the Mo isotopes become more deformed, the behavior of the proton pair gap is counter-intuitive at first sight. However, Δ_p is affected by a lowering of the level density with increasing deformation due to a shell gap that occurs at $Z = 38$ for deformations near $\epsilon_2 = 0.4$ [48]. It is probably fortuitous that $g(2_1^+)$ in ^{94}Mo is so well predicted by this collective model since other features of the level spectrum have a clear single-particle nature.

C. Interacting Boson Model Calculations

We have seen that the shell model calculations with two-body interactions, that imply a weak coupling between the proton and neutron excitations in the valence space, can qualitatively explain the sharp fall in $g(2_1^+)$ between the $N = 50$ isotope ^{92}Mo and the $N = 52$ isotope ^{94}Mo. In addition, the trends in the $g(2_1^+)$ values between ^{94}Mo and ^{104}Mo are well described by the collective model with microscopic pairing corrections based on the Migdal approximation. We now consider another approach to collective excitations with microscopic connections, in terms of the interacting boson model.

We have reproduced the bosonic configuration mixing calculations performed within the IBM-2 by Sambataro and Molnar [13] using the code NPBOS [49]. The goal was to assess whether the mixing of different configurations in the ground states of ^{98}Mo and ^{100}Mo, which was shown by Sambataro and Molnar [13] to reproduce the low-energy levels and $E2$ transition probabilities in the transitional Mo isotopes, could account for the regular increase in $g(2_1^+)$ values up to $A = 100$. Taking boson g factors $g_\nu = 0.0$ and $g_\pi = 1.0$, the g factors for the first excited 2^+ states in $^{96-104}$Mo were calculated. The resulting g factors do indeed follow the trend in the adopted values for the Mo g factors reported here, and a maximum $g(2_1^+)$ value is predicted for ^{98}Mo. A better correspondence between data and the g factors extracted from the IBM-2 mixing calcuations is attained by considering $g_\nu = 0.05$ and $g_\pi = 1.0$ as proposed by Halse [50] for this region (see Fig. 6).

For completeness, we also reproduced the IBM-2 calculations of Dejbakhsh *et al.* [16] using NPBOS to test if the alternative approach of considering $\epsilon_\nu \neq \epsilon_\pi$ could reproduce the measured Mo g factors. Using effective boson g factors $g_\nu = 0.0$ and $g_\pi = 1.0$, the results for both the $N_\pi = 2$ and $N_\pi = 4$ calculations are shown in Fig. 6. Although it was demonstrated that this approach was able to reproduce the low-energy level structure and $B(E2)$ data for the even-even Mo isotopes in the range $A = 96 - 104$, the trend in the measured 2_1^+ g factors is not reproduced.

V. SUMMARY

The gyromagnetic ratios of the first 2^+ states in the stable, even-even molybdenum isotopes have been measured using the transient field method. The present g factors compare favorably with earlier measurements by Häusser et al. [18,19], however, a steady increase in the $g(2_1^+)$ values between ^{94}Mo and ^{100}Mo is observed that was not apparent in the older measurements.

The Migdal-corrected geometrical model, successful in mapping the trends in $g(2_1^+)$ values of collective nuclei in the rare-earth region, also reproduces well the adopted $g(2_1^+)$ values for the even-even Mo isotopes with $A \geq 94$ discussed here.

The results of shell model calculations using a very restricted basis outside a ^{90}Zr core track well the moments of the nearly pure $\pi(1g_{9/2})^2_{8^+}$ configurations in ^{92,94}Mo. This simple calculation, however, underpredicts the g factors of low-spin states in ^{94,95,96}Mo. The extension of the shell model calculations to include more valence orbitals better reproduces the experimental $g(2^+)$ values near $N = 50$. Although the 2_1^+ magnetic moments are nearer to Z/A than predicted from the shell model, the collective contributions are not dominant near $N = 50$, supporting a picture in which the valence proton and neutron spaces are weakly coupled. However, as one adds neutrons beyond $N = 56$, the $\nu 1g_{7/2}$ – $\pi 1g_{9/2}$ neutron–proton interaction becomes significant. Khasa *et al.* [11] predicted that the $\pi 2p_{1/2}$ orbital is completely empty except for ^{92}Mo and ^{90}Zr, and that for $^{100-106}$Mo the valence protons are equally distributed between the $2d_{5/2}$ and $1g_{9/2}$ orbitals. Indeed the IBM-2 calculations with configuration mixing support such a picture, where the ground state of ^{98}Mo is a mixed two proton particle and four proton particle - two proton hole configuration and the ground state of ^{100}Mo is predominately of four proton particle – two proton hole character.

Finally, we draw attention to the similarity in the trends observed for $g(2_1^+)$ in the molybdenum isotopes as neutron pairs are added to ^{92}Mo and the trends displayed for $g(2_1^+)$ in the $^{142-150}$Nd isotopes, where neutrons are added to the $N = 82$ nucleus ^{142}Nd [51]. The sharp fall in $g(2_1^+)$ between the closed neutron shell nuclei (^{92}Mo and ^{142}Nd) and those with two valence neutrons (^{94}Mo and ^{144}Nd) evidently originates from the weak coupling of the proton and neutron valence spaces, noted above. However the spin dependence of the g factors in ^{94}Mo and ^{144}Nd is expected to be different: $g(8_1^+)$ in ^{94}Mo is relatively large and positive due to its dominant $\pi(g_{9/2})^2$ configuration, while $g(6_1^+)$ in ^{144}Nd is negative, originating from a predominantly $\nu(f_{7/2})^2$ configuration. It would be of considerable interest to measure the g factors as a function of spin in the Mo isotopes near $N = 50$ since the shell model predicts that there are strong variations in the spin-dependence of the g factors due to competition between the available proton and neutron configurations.

VI. ACKNOWLEDGMENTS

We would like to thank Dr. T. Kibédi and Dr. A.P. Byrne for assistance with data collection and analysis and Dr. B.A. Brown for assistance with the shell model calculations using OXBASH. The measurement of the magnetization of the Fe foil was performed at Rutgers University by T. Mertzimekis. This work was supported in part by the National Science Foundation Grant No. PHY95-28844, and the Australian Academy of Science International Exchange Program. Foreign travel support was provided by the National Science Foundation under the US-Australia Cooperative Research Program, Grant No. PHY99-73201. PFM, DEG, and JIP would like to acknowledge the hospitality of the Nuclear Physics Department, Research School of Physical Sciences and Engineering, Australian National University during the completion of these measurements.

REFERENCES

[1] W. Gelletly, M.A. Bentley, H.G. Price, J. Simpson, C.J. Gross, J.L. Durell, B.J. Varley, O. Skeppstedt, and S. Rastikerdar, Phys. Lett. B **253**, 287 (1991).

[2] I. Talmi and I. Unna, Nucl. Phys. **19**, 225 (1960).

[3] N. Auerbach and I. Talmi, Nucl. Phys. **64**, 458 (1965).

[4] J. Vervier, Nucl. Phys. **75**, 17 (1966).

[5] D.H. Gloeckner, Nucl. Phys. **A253**, 301 (1975).

[6] Chang-hua Zhang, Shun-jin Wang and Jin-nan Gu, Phys. Rev. C **60**, 054316 (1999).

[7] A. Holt, T. Engeland, M. Hjorth-Jensen and E. Osnes, Phys. Rev. C **61**, 064318 (2000).

[8] I.P. Johnstone and I.S. Towner, Eur. Phys. J. A **2**, 263 (1998).

[9] A.F. Lisetskiy, N. Pietralla, C. Fransen, R.V. Jolos and P. von Brentano, Nucl. Phys. **A677**, 100 (2000).

[10] P. Federman and S. Pittel, Phys. Lett. **77B**, 29 (1978).

[11] S.K. Khasa, P.N. Tripathi, and S.K. Sharma, Phys. Lett. **119B**, 257 (1982).

[12] K. Heyde, J. Jolie, J. Moreau, J. Ryckebusch, M. Waroquier, P. van Duppen, M. Huyse, J.L. Wood, Nucl. Phys. **A466**, 189 (1987).

[13] M. Sambataro and G. Molnar, Nucl. Phys. **A376**, 201 (1982).

[14] G. Cata, D. Bucurescu, D. Cutoiu, M. Ivascu, and N.V. Zamfir, Z. Phys. A**335**, 271 (1990).

[15] R.F. Casten, Nucl. Phys. **A443**, 1 (1985).

[16] H. Dejbakhsh, D. Latypov, G. Ajupova, and S. Shlomo, Phys. Rev. C**46**, 2326 (1992).

[17] G.M. Heestand, R.R. Borchers, B. Herskind, L. Grodzins, R. Kalish, and D.E. Murnick, Nucl. Phys. **A133**, 310 (1969).

[18] O. Häusser, Lecture Notes in Physics **92**, ed. B.A. Robson (Springer-Verlag, Berlin, 1979), p. 68.

[19] O. Häusser, B. Haas, J.F. Sharpey-Schafer, D. Ward, and H.R. Andrews, AECL-6366 (1978) p. 19.

[20] G. Menzen, A. Wolf, H. Lawin, G. Lhersonneau, and K. Sistemich, Z. Phys. A**321**, 593 (1985).

[21] W. Greiner, Nucl. Phys. **80**, 417 (1966).

[22] N. Benczer-Koller, M. Hass, and J. Sak, Ann. Rev. Nucl. Part. Sci. **30**, 53 (1980).

[23] J.F. Ziegler, J.P. Biersack, and U. Littmark, The stopping and range of ions in solids, in: The stopping and ranges of ions in matter, Vol. 1, ed. J.F. Ziegler (Permagon, New York, 1985).

[24] N.K.B. Shu, D. Melnick, J.M. Brennan, W. Semmler, and N. Benczer-Koller, Phys. Rev. C**21**, 1828 (1980).

[25] H.R. Andrews, O. Häusser, D. Ward, P. Taras, R. Nicole, J. Keinonen, P. Skensved, and B. Haas, Nucl. Phys. **A282**, 509 (1982).

[26] A.E. Stuchbery, C.G. Ryan, H.H. Bolotin, and S.H. Sie, Phys. Rev. C**23**, 1618 (1981).

[27] A. Piqué, J.M. Brennan, R. Darling, R. Tanczyn, D. Ballon and N. Benczer-Koller, Nucl. Instrum. Methods Phys. Res. A **279**, 579 (1989).

[28] A. Winther and J. de Boer, Coulomb Excitation, eds. K. Alder and A. Winther (Academic Press, New York, 1966) p. 303.

[29] P. Paradis, G. Lamoureux, R. Leconte, and S. Monaro, Phys. Rev. C**14**, 835 (1976).

[30] S. Raman, C.H. Malarkey, W.T. Milner, C.W. Nester, Jr., and P.H. Stelson, At. Data Nucl. Data Tables **36**, 1 (1987).
[31] G.J. Lampard, H.H. Bolotin, C.E. Doran, L.D. Wood, I. Morrison, and A.E. Stuchbery, Nucl. Phys. **A496**, 589 (1989).
[32] K. Johansson, E. Karlsson, L.O. Norlin, R.Å. Windah, and M.R. Ahmed, Nucl. Phys. **A188**, 600 (1972).
[33] V. Singh, J. Phys. Soc. Japan **29**, 1111 (1970).
[34] J.M. Brennan, M. Hass, N.K.B. Shu, and N. Benczer-Koller, Phys. Rev. C**21**, 574 (1980).
[35] D. De Frenne, E. Jacobs, and M. Verboven, Nucl. Data Sheets **45**, 363 (1985).
[36] D. De Frenne, E. Jacobs, M. Verboven, and G. De Met, Nucl. Data Sheets **53**, 73 (1988).
[37] R.H. Dean and G.A. Jakins, J. Phys. F (London) **8**, 1563 (1978).
[38] L. Kisslinger and R. Sorenson, Rev. Modern Phys. **35**, 853 (1963).
[39] R.J. Lombard, Nucl. Phys. **A114**, 449 (1968).
[40] A.B. Migdal, Nucl. Phys. **13**, 655 (1959).
[41] P. Raghavan, At. Data Nucl. Data Tables, **42**, 189 (1989).
[42] I. Berkes, M. De Jésus, B. Hlimi, M. Massaq, E.H. Sayouty and K. Heyde, Phys. Rev. C **44**, 104 (1991).
[43] G. Jakob, N. Benczer-Koller, J. Holden, G. Kumbartzki, T.J. Mertzimekis, K.-H. Speidel, C.W. Beausang and R. Krücken, Phys. Lett. B **468**, 13 (1999).
[44] A. Etchegoyen, W.D. Rae, N.S. Godwin, W.A. Richter, C.H. Zimmerman, B.A. Brown, W.E. Ormand, and J.S. Winfield, Computer code OXBASH, MSU-NSCL Report No. 524, 1985 (unpublished).
[45] A.E. Stuchbery, Nucl. Phys. **A 589**, 222 (1995).
[46] P.B. Semmes and I. Ragnarsson, The particle + triaxial rotor model. A user's guide, (unpublished). Distributed at the Hands-on nuclear theory workshop, Oak Ridge (5-16 August 1991), and references therein.
[47] P. Möller and J.R. Nix, At. Data Nucl. Data Tables **35**, 15 (1986).
[48] T. Bengtsson and I. Ragnarsson, Nucl. Phys. **A 436**, 14 (1985).
[49] O. Scholten, Ph.D. Thesis, University of Groningen, 1980.
[50] P. Halse, J. Phys. G **19**, 1859 (1993).
[51] J. Holden, N. Benczer-Koller, G. Jakob, G. Kumbartzki, T.J. Mertzimekis, K.-H. Speidel, C.W. Beausang, R. Krücken, A. Macchiavelli, M. McMahan, L. Phair, A. E. Stuchbery, P. Maier-Komor, W. Rogers and A.D. Davies, Phys. Lett. **B**, in press.

TABLES

TABLE I. Kinematics and predicted transient field strengths for Mo in Fe.

Isotope	$\langle E_i \rangle$ [a]	$\langle E_e \rangle$ [a]	$\langle v_i/v_0 \rangle$ [a]	$\langle v_e/v_0 \rangle$ [a]	$\langle v/v_0 \rangle$ [a]	$-\phi_{RU}$ [b]	$-\phi_{CR}$ [c]	$-\phi_{Pd}$ [d]	$-\phi_{adopted}$ [e]
^{92}Mo	63.8	11.3	5.29	2.22	3.49	24.2	24.8	20.5	22.7
^{94}Mo	63.4	11.4	5.21	2.21	3.45	34.5	35.2	29.3	32.5
^{96}Mo	62.9	11.6	5.14	2.20	3.42	35.2	35.8	30.1	32.9
^{98}Mo	62.5	11.7	5.07	2.19	3.39	35.3	36.0	30.1	32.9
^{100}Mo	62.1	11.8	5.00	2.18	3.35	36.8	37.3	31.3	34.0

[a] Average energies with which the Mo ions enter into (exit from) the Fe foil, $\langle E_i \rangle$ ($\langle E_e \rangle$), the corresponding ion velocities, $\langle v_i/v_0 \rangle$ ($\langle v_e/v_0 \rangle$), and the average ion velocity whilst in the Fe layer, $\langle v/v_0 \rangle$. $v_0 = c/137$ is the Bohr velocity. These quantities were calculated with the stopping powers of Ziegler *et al.* [23].

[b] The integral transient-field strength, see Eq. 2, predicted by the Rutgers parametrization [24].

[c] The integral transient-field strength, see Eq. 2, predicted by the Chalk River parametrization [25].

[d] The integral transient-field strength, see Eq. 2, predicted by a parametrization which fits transient field data for Pd in Fe [26].

[e] The integral transient-field strength adopted for Mo in Fe which takes into account data on Rh and Pd in Fe presented in Table III; see the text.

TABLE II. Measured counting ratios, S values, and precession angles from the forward and backward detector pairs for the $2_1^+ \rightarrow 0_1^+$ transition in each stable, even-even Mo isotope.

	Forward			Backward			
Isotope	ϵ ($\times 10^3$)	S	$\Delta\theta$ (mrad)[a]	ϵ ($\times 10^3$)	S	$\Delta\theta$ (mrad)[a]	$\langle \Delta\theta \rangle$ (mrad)
^{92}Mo	$+88 \pm 41$	-2.71	-32 ± 15	-72 ± 53	$+2.88$	-25 ± 18	-29 ± 12
^{94}Mo	$+23.6 \pm 8.7$	-2.65	-8.9 ± 3.3	-24.9 ± 9.4	$+2.81$	-8.9 ± 3.4	-8.9 ± 2.4
^{96}Mo	$+31.7 \pm 3.2$	-2.36	-13.4 ± 1.4	-35.9 ± 4.5	$+2.50$	-14.4 ± 1.9	-13.8 ± 1.1
^{98}Mo	$+40.5 \pm 3.4$	-2.47	-16.4 ± 1.5	-38.4 ± 4.7	$+2.62$	-14.7 ± 1.9	-15.7 ± 1.2
^{100}Mo	$+34.4 \pm 2.8$	-2.03	-16.9 ± 1.5	-40.5 ± 4.4	$+2.16$	-18.7 ± 2.1	-17.5 ± 1.2

[a] The error on $\Delta\theta$ contains a 3% systematic error associated with the derived slope of the $2^+ \rightarrow 0^+$ angular correlation (S values).

TABLE III. Transient field strengths for ^{106,108,110}Pd and ^{103}Rh.

Isotope	J_i^π	$-\Delta\theta$ (mrad)[a]	g	$-\phi_{\rm exp}$	$-\phi_{\rm calc}$ [b]	$\phi_{\rm exp}/\phi_{\rm calc}$
^{106}Pd	2_1^+	16.1 ± 1.1	0.402 ± 0.017 [d]	40.1 ± 3.2		
^{108}Pd	2_1^+	13.9 ± 1.1	0.36 ± 0.03 [e]	38.6 ± 4.4		
^{110}Pd	2_1^+	12.4 ± 1.5	0.31 ± 0.03 [e]	40.0 ± 6.2		
				$\langle 39.6 \pm 2.4 \rangle$ [c]	40.34	0.982 ± 0.059
^{103}Rh	$3/2_1^-$	21.2 ± 1.4	0.69 ± 0.13 [f]	30.7 ± 6.1	36.11	0.85 ± 0.17
^{103}Rh	$5/2_1^-$	16.8 ± 0.8	0.435 ± 0.018 [f]	38.6 ± 2.4	36.94	1.045 ± 0.066
						1.000 ± 0.043[g]

[a]From Ref. [31].
[b]Transient field calculation using Eq. 6 with $a = 23.65$ T and $p = 0.41$; see text.
[c]Weighted average of $\phi_{\rm exp}$ for ^{106,108,110}Pd.
[d]Weighted average of g factors from Ref. [32] and Ref. [33]. g factors were re-evaluted using $\tau(2_1^+)$ from Ref. [36].
[e]From Ref. [34].
[f]From Ref. [35].
[g]Average value.

TABLE IV. Integral transient field strengths and absolute g factors for the 2_1^+ states in ^{92,94,96,98,100}Mo.

Isotope	J_i^π	τ (ps) [a]	$\Delta\theta$ (mrad)	ϕ [b]	$g^{\rm c}$
^{92}Mo	2_1^+	0.537 ± 0.033	-29 ± 12	-22.66 ± 1.09	$1.28 \pm 0.53 \pm 0.53$
^{94}Mo	2_1^+	4.00 ± 0.08	-8.9 ± 2.4	-32.45 ± 1.39	$0.274 \pm 0.074 \pm 0.075$
^{96}Mo	2_1^+	5.27 ± 0.10	-13.8 ± 1.1	-32.92 ± 1.41	$0.419 \pm 0.033 \pm 0.038$
^{98}Mo	2_1^+	5.04 ± 0.09	-15.7 ± 1.2	-32.86 ± 1.40	$0.478 \pm 0.037 \pm 0.042$
^{100}Mo	2_1^+	17.89 ± 0.35	-17.5 ± 1.2	-33.99 ± 1.45	$0.515 \pm 0.035 \pm 0.042$

[a]Lifetimes taken from Ref. [30].
[b]ϕ evaluated from Eq. 2 with the transient field parametrized by Eq. 6 with $a = 23.65 \pm 1.01$ T and $p = 0.41$ (see text).
[c]$g = \Delta\theta/\phi$. The first error, from the statistical error in the measured precession alone, represents the error in the relative g factors; the second, which includes the uncertainty in the field calibration, represents the error in the absolute g factors.

TABLE V. Re-evaluation of previous even-even Mo g factor measurements [18,19].

Isotope	$\langle v_i/v_0\rangle$ [a]	L_{Fe} (mg/cm^2)	$\langle v_e/v_0\rangle$ [b]	$\Delta\theta$ (mrad)	ϕ [c]	g[d]
^{92}Mo	6.19	3.95	1.67	-32.7 ± 2.0	-28.63 ± 1.22	$1.14 \pm 0.09 \pm 0.14$
^{94}Mo	5.94	3.58	1.87	-14.1 ± 1.5	-43.35 ± 1.85	$0.325 \pm 0.037 \pm 0.053$
^{96}Mo	6.17	3.70	2.01	-15.4 ± 1.4	-44.21 ± 1.89	$0.348 \pm 0.035 \pm 0.052$
^{98}Mo	6.20	3.75	2.01	-22.2 ± 1.7	-44.87 ± 1.92	$0.495 \pm 0.043 \pm 0.067$
^{100}Mo	5.87	3.96	1.69	-21.2 ± 1.4	-52.53 ± 2.24	$0.404 \pm 0.032 \pm 0.052$

[a]Average ion velocity entering the Fe foil taken from Ref. [19]. $v_0 = c/137$ is the Bohr velocity.
[b]Average ion velocity exiting the Fe foil calculated using the stopping powers of Ziegler *et al.* [23]. $v_0 = c/137$ is the Bohr velocity
[c]ϕ evaluated from Eq. 2 with the transient field parametrized by Eq. 6 with $a = 23.65 \pm 1.01$ T and $p = 0.41$ (see text).
[d]First error includes uncertainty in the measured precession and the transient field strength, the second includes an estimate of the potential systematic error introduced through use of different targets for each isotope.

TABLE VI. Adopted g factors for the 2_1^+ states of even-even Mo isotopes.

Isotope	$E(2_1^+)$ (keV)	g factor			
		Ref. [18,19]		present	adopted
		as reported	recalibrated [a]		
^{92}Mo	1509	$+1.07 \pm 0.19$	$+1.14 \pm 0.14$	$+1.28 \pm 0.53$	$+1.15 \pm 0.14$
^{94}Mo	871	$+0.33 \pm 0.06$	$+0.325 \pm 0.053$	$+0.274 \pm 0.075$	$+0.308 \pm 0.043$
^{96}Mo	778	$+0.34 \pm 0.05$	$+0.348 \pm 0.052$	$+0.419 \pm 0.038$	$+0.394 \pm 0.031$
^{98}Mo	787	$+0.49 \pm 0.08$	$+0.495 \pm 0.067$	$+0.478 \pm 0.042$	$+0.483 \pm 0.036$
^{100}Mo	536	$+0.43 \pm 0.06$	$+0.404 \pm 0.052$	$+0.515 \pm 0.042$	$+0.471 \pm 0.033$
^{102}Mo	297				$+0.42 \pm 0.07$ [b]
^{104}Mo	192				$+0.19^{+0.12}_{-0.11}$ [b]

[a]See Table V and text.
[b]Ref. [20].

TABLE VII. Shell model calculations of moments in Zr isotopes.

Isotope (J^π)	Quantity	Experiment [a]	Theory I [b]	Theory II [c]	Theory III [d]
^{90}Zr (5^-)	E_x	2319		2221	2847
	g	$+1.25 \pm 0.03$		+1.213	+1.084
^{90}Zr (8^+)	E_x	3589		3473	3797
	g	$+1.356 \pm 0.007$		+1.355	+1.295
	Q	51 ± 3^e		−45	−60
	$B(\mathrm{E2};\, 8_1^+ \rightarrow 6_1^+)$	57 ± 4		52	46
^{91}Zr ($5/2^+$)	E_x	0	0	0	
	g	-0.521448 ± 0.000001	−0.574	−0.557	−0.555
	Q	-21 ± 1	−18	−22	−23
^{91}Zr ($15/2^-$)	E_x	2288		2019	2882
	g	$+0.70 \pm 0.01$		+0.617	+0.594
^{91}Zr ($21/2^+$)	E_x	3167		3141	3476
	g	$+0.935 \pm 0.008$		+0.895	+0.868
	Q	-86 ± 5		−62	−96
^{92}Zr (2^+)	E_x	934	934	878	979
	g	-0.180 ± 0.010	−0.574	−0.444	−0.388
^{92}Zr (4^+)	E_x	1495	1495	1526	1595
	g	-0.50 ± 0.11	−0.574	−0.548	−0.436
^{94}Zr (2^+)	E_x	919	934	885	
	g	-0.329 ± 0.015	−0.574	−0.537	
	$B(\mathrm{E2};\, 2_1^+ \rightarrow 0_1^+)$	112 ± 13	71	123	
	$B(\mathrm{E2};\, 4_1^+ \rightarrow 2_1^+)$	22.6 ± 0.6	49	46	
^{95}Zr ($5/2^+$)	E_x	0	0	0	
	g	0.452 ± 0.008^e	−0.574	−0.571	
^{96}Zr (2^+)	E_x	1750		1927	
	g			−0.082	

[a] E_x is the excitation energy in keV, g is the gyromagnetic ratio from Refs. [41–43], Q is the quadrupole moment in fm^2, and the $B(E2)\downarrow$ values have units e^2fm^4.

[b] ^{90}Zr core with $\pi 1g_{9/2}$ and $\nu 2d_{5/2}$. Missing entries indicate states outside the model space.

[c] ^{88}Sr core with $\pi(2p_{1/2},\, 1g_{9/2})$ and $\nu(2d_{5/2},\, 3s_{1/2})$.

[d] ^{66}Ni core with $\pi(1f_{5/2},\, 2p_{3/2},\, 2p_{1/2},\, 1g_{9/2})$ and ν $(1g_{9/2},\, 2p_{1/2},\, 2d_{5/2},\, 3s_{1/2},\, 2d_{3/2},\, 1g_{7/2})$; no more than 2 proton holes are allowed in $\pi(1f_{5/2},\, 2p_{3/2})$ and the neutron orbits ν $(1g_{9/2},\, 2p_{1/2})$ are

filled. This calculation was not performed for $^{94,95,96}Zr$.

[e] The sign of Q or g has not been determined experimentally.

Isotope (J^π)	Quantity	Experiment [a]	Theory I [b]	Theory II [c]	Theory III [d]
^{92}Mo (2^+)	E_x	1509	1509	1457	1489
	g	$+1.15 \pm 0.14$	$+1.354$	$+1.354$	$+1.315$
	$B(\mathrm{E2};\, 2_1^+ \to 0_1^+)$	212 ± 10	165	182	209
^{92}Mo (8^+)	E_x	2761	2761	2642	2652
	g	$+1.413 \pm 0.006$	$+1.355$	$+1.355$	$+1.350$
	Q	-34	-45	-38	-36
	$B(\mathrm{E2};\, 8_1^+ \to 6_1^+)$	32 ± 1	52	39	35
^{94}Mo (2^+)	E_x	871	919	838	853
	g	$+0.308 \pm 0.043$	-0.439	$+0.185$	$+0.226$
	Q	-13 ± 8 or $+1 \pm 8$	$+17$	$+22$	$+23$
	$B(\mathrm{E2};\, 2_1^+ \to 0_1^+)$	391 ± 5	188	319	340
^{94}Mo (8^+)	E_x	2956	2759	2776	2628
	g	$+1.308 \pm 0.009$	$+1.345$	$+1.307$	$+1.298$
	Q	47 ± 1[e]	-48	-57	-61
^{95}Mo ($5/2^+$)	E_x	0	0	0	
	g	-0.36568 ± 0.00004	-0.562	-0.417	
	Q	-2.2 ± 0.1	$+0.8$	$+2.1$	
^{95}Mo ($3/2^+$)	E_x	204	250	152	
	g	-0.263 ± 0.006	-0.563	-0.448	
^{96}Mo (2^+)	E_x	778	927	920	
	g	$+0.394 \pm 0.031$	-0.492	$+0.071$	
	Q	-20 ± 8 or $+4 \pm 8$	-11	-2	
	$B(\mathrm{E2};\, 2_1^+ \to 0_1^+)$	540 ± 8	137	362	

TABLE VIII. Shell model calculations of moments in Mo isotopes.

[a] E_x is the excitation energy in keV, g is the gyromagnetic ratio from present work and Ref. [41], Q is the quadrupole moment in fm^2, and the $B(E2)\downarrow$ values have units e^2fm^4.

[b] ^{90}Zr core with $\pi 1g_{9/2}$ and $\nu 2d_{5/2}$.

[c] ^{88}Sr core with $\pi(2p_{1/2}, 1g_{9/2})$ and $\nu(2d_{5/2}, 3s_{1/2})$.

[d] ^{66}Ni core with $\pi(1f_{5/2}, 2p_{3/2}, 2p_{1/2}, 1g_{9/2})$ and ν $(1g_{9/2}, 2p_{1/2}, 2d_{5/2}, 3s_{1/2}, 2d_{3/2}, 1g_{7/2})$; no more than 2 proton holes are allowed in $\pi(1f_{5/2}, 2p_{3/2})$ and the neutron orbits ν $(1g_{9/2}, 2p_{1/2})$ are filled. This calculation was not performed for ^{95,96}Mo.

[e] The sign of Q has not been determined experimentally.

TABLE IX. Deformations, pair gaps and gyromagnetic ratios in even-even Mo isotopes.

Nucleus	β_2[a]	ε_2[a]	Δ_p (keV)	Δ_n (keV)	g theory	g experiment[b]
^{94}Mo	0.01	0.01	1148	989	0.345	0.308 ± 0.043
^{96}Mo	0.09	0.09	1144	1217	0.428	0.394 ± 0.031
^{98}Mo	0.17	0.16	1060	1219	0.445	0.483 ± 0.036
^{100}Mo	0.22	0.20	966	1301	0.483	0.471 ± 0.033
^{102}Mo	0.32	0.28	823	1239	0.479	0.42 ± 0.07
^{104}Mo	0.34	0.30	810	1202	0.460	$0.19^{+0.12}_{-0.11}$

[a]Estimated from Ref. [47].

[b]Adopted values from Table VI.

FIGURES

FIG. 1. Low-energy level structures of the even-even Mo isotopes. Only the known 0^+, 2^+, and 4^+ states below 2.5 MeV are shown.

FIG. 2. γ-ray spectrum for energies up to 1.7 MeV resulting from the Coulomb excitation of the $^{\rm nat}$Mo target with 100 MeV ^{32}S ions. The spectrum includes all data collected at $-65°$ for both field directions. The $2_1^+ \rightarrow 0_1^+$ transitions are labelled by isotope.

FIG. 3. Particle-γ-ray angular correlations for the $2_1^+ \rightarrow 0_1^+$ transitions in ^{94}Mo, ^{96}Mo, ^{98}Mo, and ^{100}Mo. The measured (filled circles) and calculated (solid lines) correlations are given for the γ-ray detectors in the negative and positive forward quadrants.

FIG. 4. Adopted $g(2_1^+)$ values (filled circles) as a function of neutron number for the even-even Mo isotopes compared with g factors predicted from shell model calculations using a ^{90}Zr core with valence orbitals $\pi 1g_{9/2}$ and $\nu 2d_{5/2}$ (Calculation I, dotted line), a ^{88}Sr core with valence orbitals $\pi(2p_{1/2}, 1g_{9/2})$ and $\nu(2d_{5/2}, 3s_{1/2})$ (Calculation II, dashed line), and a more extended basis space which includes $\pi(1f_{5/2}, 2p_{3/2}, 2p_{1/2}, 1g_{9/2})$ and $\nu(1g_{9/2}, 2p_{1/2}, 2d_{5/2}, 3s_{1/2}, 2d_{3/2}, 1g_{7/2})$ (Calculation III, solid line).

FIG. 5. Adopted $g(2_1^+)$ values (filled circles) as a function of neutron number for the even-even Mo isotopes. The solid line connects the g factor values from the hydrodynamical model with pairing corrections in the Migdal approximation.

FIG. 6. Adopted $g(2_1^+)$ values (filled circles) as a function of neutron number for the even-even Mo isotopes. The g factors predicted from the IBM-2 calculations with $N_\pi = 1$ and $N_\pi = 3$ mixed configurations [13] with $g_\nu = 0.05$, $g_\pi = 1.0$ are connected by the solid line. The dot-dashed and dotted lines connect the g factor values calculated using the IBM-2 parametrization of Dejbakhsh *et al.* [16] for $N_\pi = 2$ and $N_\pi = 4$, respectively.

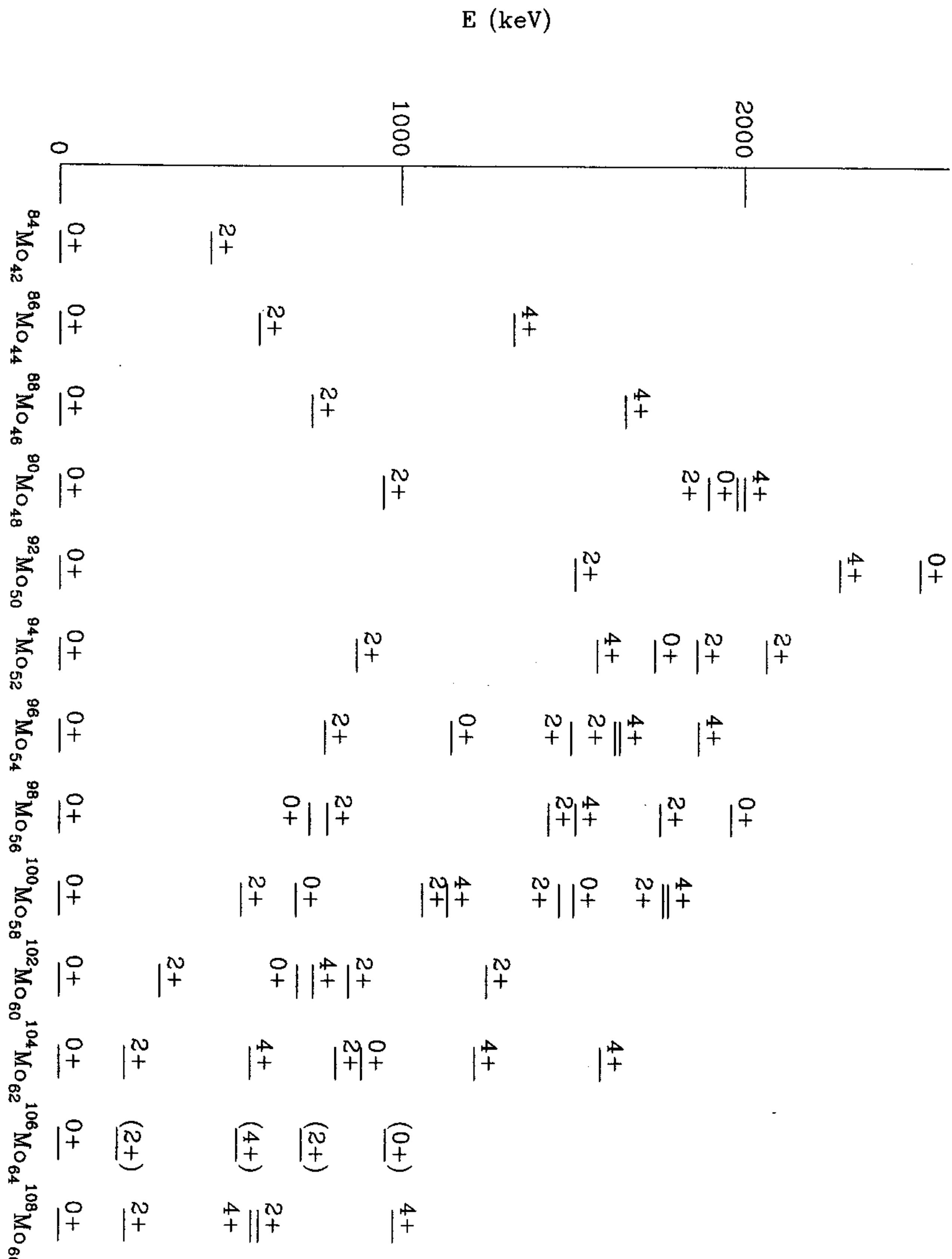
E (keV)
0
1000
2000
$^{84}Mo_{42}$
$^{86}Mo_{44}$
$^{88}Mo_{46}$
$^{90}Mo_{48}$
$^{92}Mo_{50}$
$^{94}Mo_{52}$
$^{96}Mo_{54}$
$^{98}Mo_{56}$
$^{100}Mo_{58}$
$^{102}Mo_{60}$
$^{104}Mo_{62}$
$^{106}Mo_{64}$
$^{108}Mo_{66}$

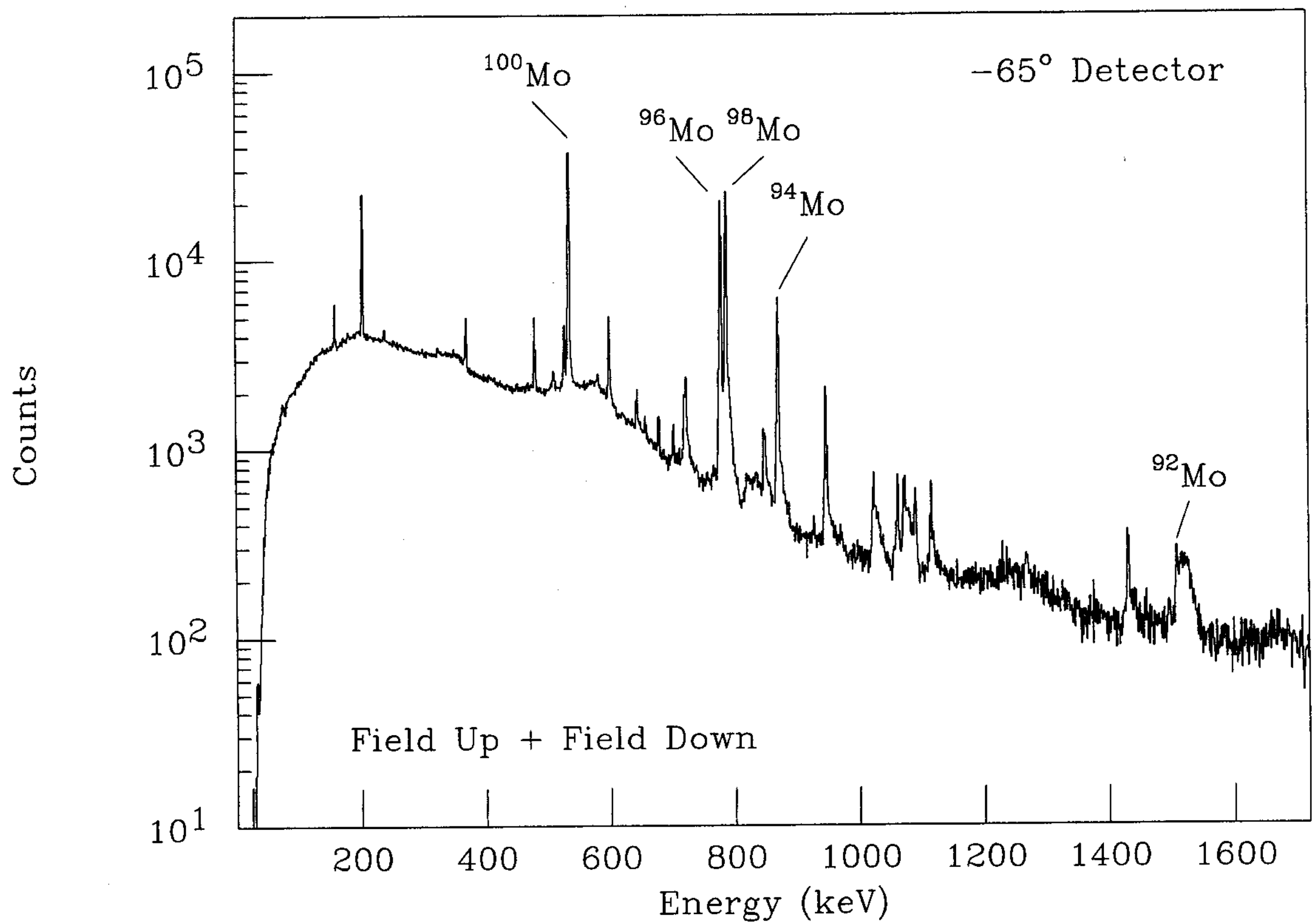

Counts
10^5
10^4
10^3
10^2
10^1
^{100}Mo
^{96}Mo ^{98}Mo
^{94}Mo
^{92}Mo
−65° Detector
Field Up + Field Down
200
400
600
800
1000
1200
1400
1600
Energy (keV)

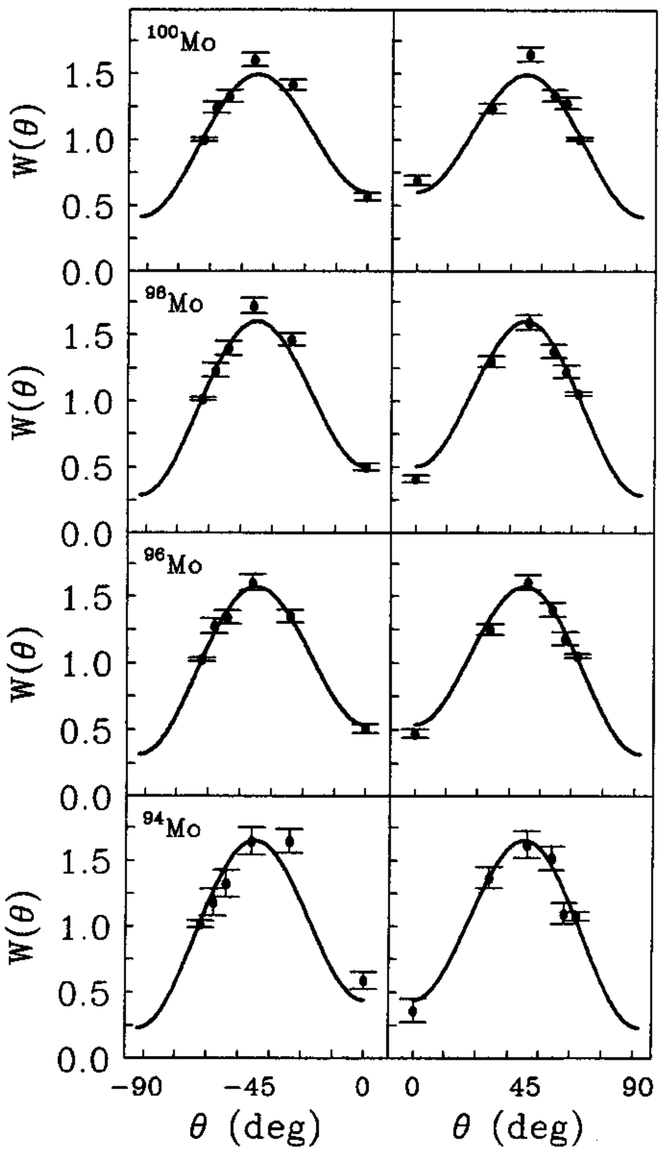

^{100}Mo
^{98}Mo
^{96}Mo
^{94}Mo
W(θ)
0.0
0.5
1.0
1.5
−90
−45
0
45
90
θ (deg)

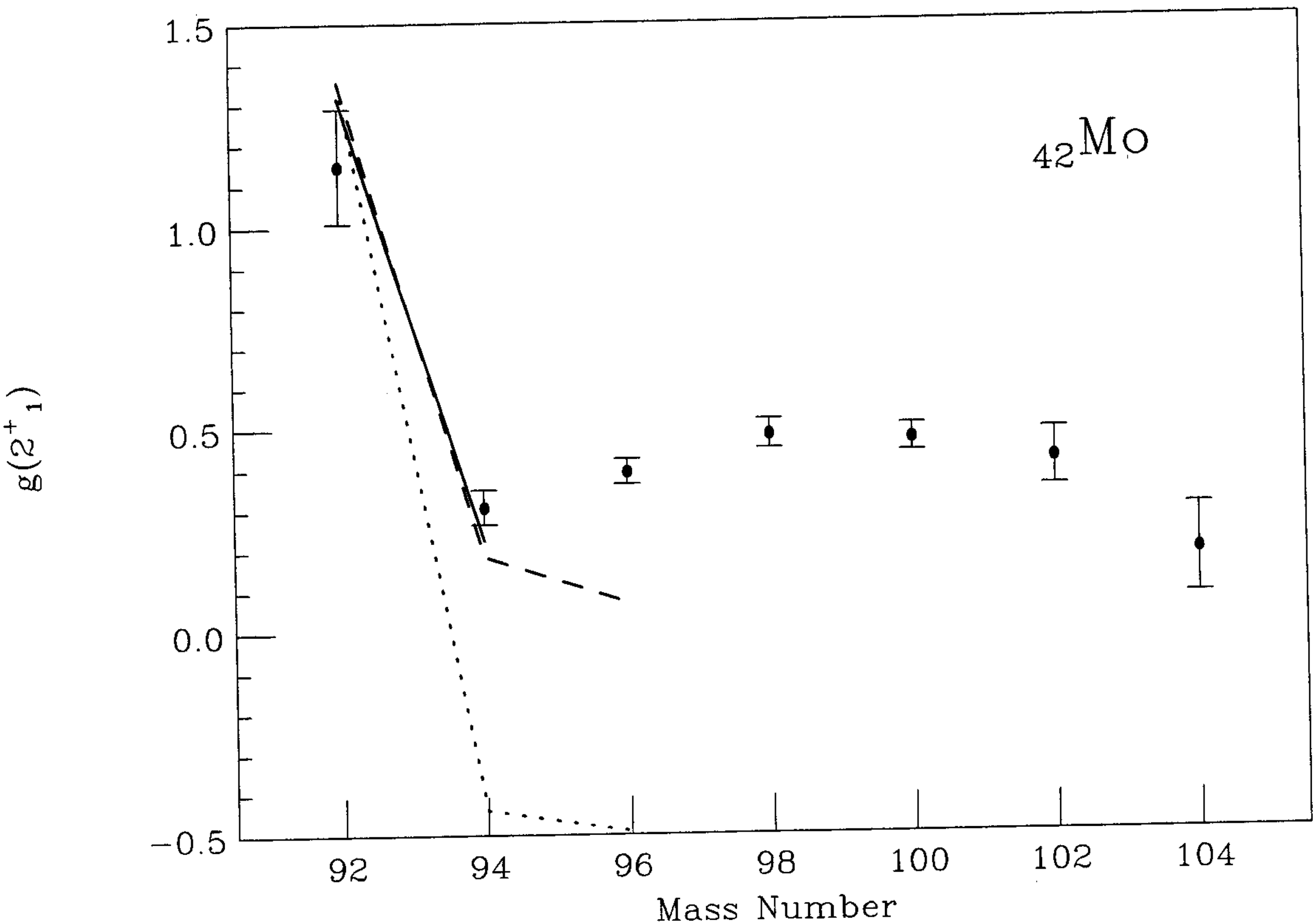

1.5
1.0
0.5
0.0
−0.5
g(2+1)
42Mo
92
94
96
98
100
102
104
Mass Number

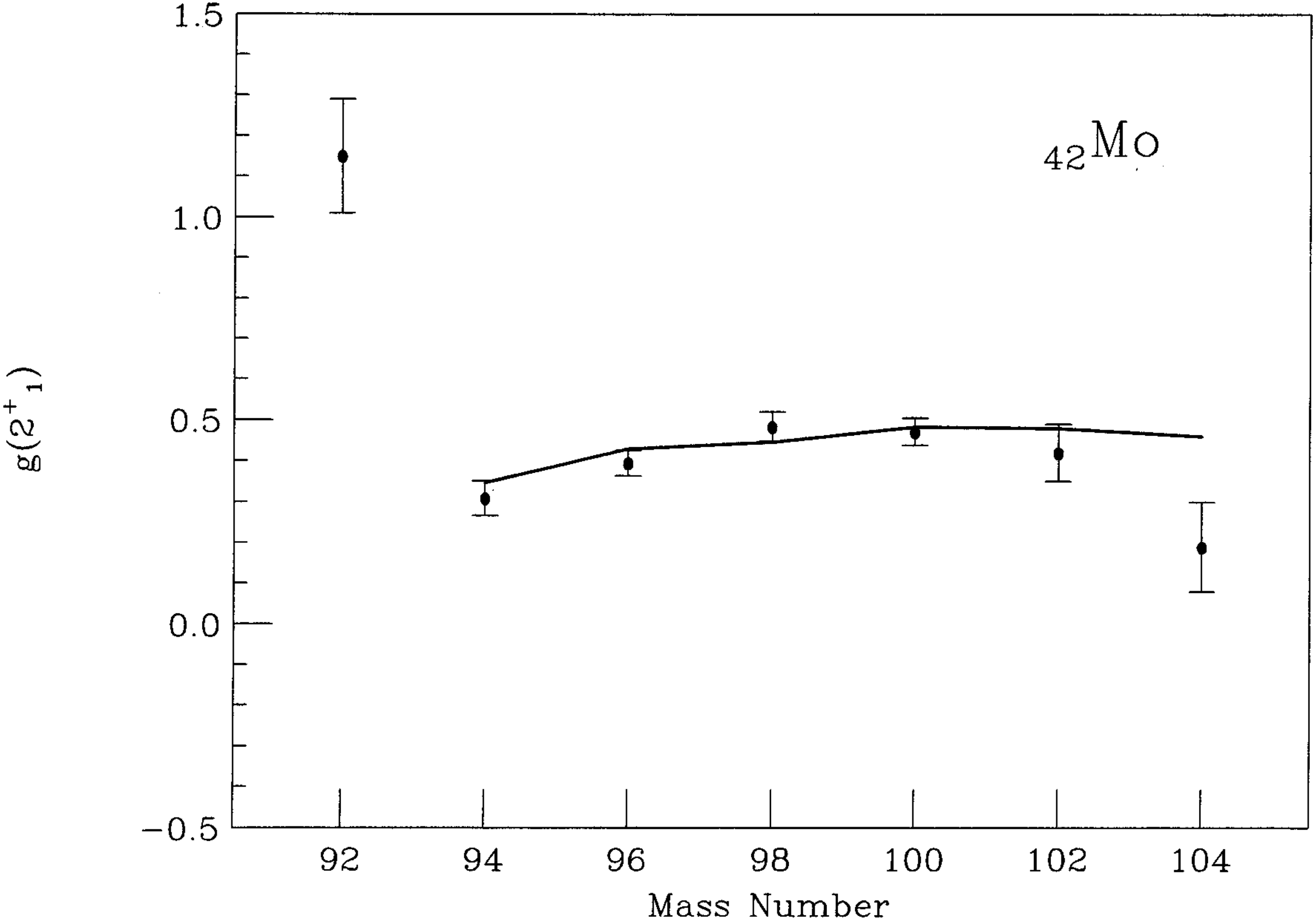

42Mo
g(2+1)
1.5
1.0
0.5
0.0
−0.5
92
94
96
98
100
102
104
Mass Number

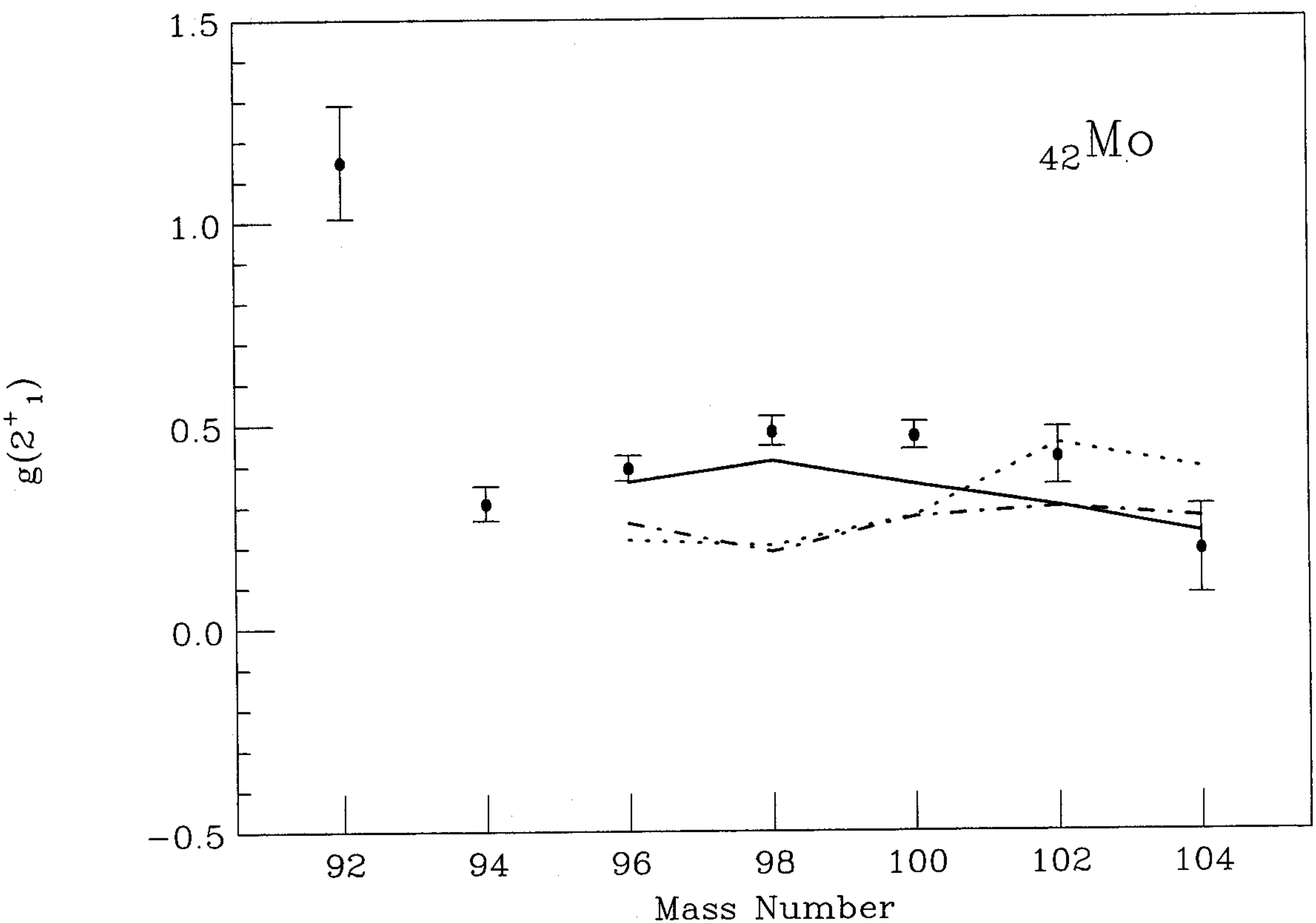

$_{42}$Mo
$g(2^+_1)$
1.5
1.0
0.5
0.0
−0.5
92
94
96
98
100
102
104
Mass Number